Journal of Petroleum Science and Technology 14(3): 43, 2024, Pages 2-10
DOI:10.22078/jpst.2025.5614.1968

Journal of Petroleum Science and Technology
Research Paper
https://jpst.ripi.ir/

Fabrication of Carbon Molecular Sieve with KOH Activated Olive Kernels for the Separation of Carbon Dioxide from Methane Gas

Hamid Reza Bozorgzadeh
Research Institute of Petroleum Industry, (RIPI) Tehran, Iran

Abstract
In this study, the synthesis of adsorbents from agricultural residues, specifically olive kernels, was examined using chemical precipitation with potassium hydroxide (KOH) as the activating agent. The carbonization process was conducted under an inert gas atmosphere at three temperatures: 600°C, 700°C, and 800°C. Subsequently, a carbon molecular sieve (CMS) was developed by incorporating a binder into the activated carbon. The specific surface area of the produced samples was determined using the Brunauer-Emmett-Teller (BET) method, with measured values ranging from 360 m^2/g to a maximum of 1103 m^2/g. Moreover, the adsorption and separation characteristics of carbon dioxide (CO_2) and methane (CH_4) were evaluated for both activated carbon (AC) and carbon molecular sieves (CMS) across a pressure range of 1,200 to 1,500 kPa. Additionally, the obtained adsorption isotherms were analyzed using the Langmuir, Freundlich, and Sips models. Furthermore, a strong correlation was observed between the experimental data and the Sips isotherm, indicating enhanced selectivity for CO_2 over CH_4. Ultimately, among the investigated samples, the activated carbon subjected to carbonization at 800°C exhibited the highest CO_2 adsorption capacity, reaching 0.1699 g of CO_2 per gram of adsorbent, highlighting its potential efficacy for gas separation applications.

Keywords: Adsorption; Olive Kernel; Carbon Dioxide Removal; Carbon Molecular Sieve; Carbonization.

Introduction
Activated carbon plays a very important role in natural gas adsorption technology [1]. Recent research has focused extensively on the cost-effective production of carbon-based adsorbents. Natural gas, primarily composed of methane, is recognized as an optimal fuel choice due to its widespread availability and economic feasibility. Furthermore, its combustion generates lower emissions compared to gasoline, producing reduced levels of toxic carbon monoxide. Consequently, the purification of natural gas remains a critical process for enhancing its efficiency and environmental benefits [2]. The presence of CO_2 in biogas and natural gas contributes to global warming, diminishes the fuel's energy content, and induces system corrosion [3,-4]. Additionally, CO_2 adsorption poses a significant challenge in chemical processes. Moreover, various techniques, including boiling point distillation, amine absorption, and membrane-based methods, have been explored for carbon dioxide separation; however, their high energy demands render them economically impractical. Also, adsorption-based separation, utilizing specialized adsorbents, offers a cost-effective alternative with greater feasibility [5]. Moreover, activated carbon, characterized by its extensive surface area and substantial pore volume, is derived from various carbonaceous sources. The primary raw materials for commercial production include coal, agricultural biomass, and lignocellulosic compounds [6]. In recent years, the production of low-cost activated carbon from agricultural wastes such as olive pits [7], almond shells [8], peach pits [9], cherry pits [10], coffee [11] and corn [12] has attracted the attention of many researchers.
Olive kernels are classified as lignocellulosic materials, primarily composed of cellulose, hemicellulose, and lignin. These structural components make olive kernels a promising precursor for activated carbon production, offering desirable adsorption properties such as high mechanical strength, extensive surface area, and well-developed pore architecture. Additionally, the utilization

*Corresponding author: Hamid Reza Bozorgzadeh, Research Institute of Petroleum Industry, Tehran, Iran
E-mail addresses: bozorgzadehhr@ripi.ir
Received 2025-02-04, Received in revised form 2025-06-10, Accepted2025-07-01, Available online 2025-08-16

of this material has gained recognition in environmental protection initiatives [13].

Using KOH for the activation of AC is one of the well-known chemical methods that has attracted much attention in recent years [14, 15]. Furthermore, this study aimed to achieve the separation of CO_2 from methane using carbon molecular sieves (CMS). In addition, the carbonization process was conducted at three distinct temperatures—600 °C, 700 °C, and 800 °C—under controlled conditions. Moreover, following carbonization, activated carbon was processed to form CMS through specialized treatment. Furthermore, activation with potassium hydroxide (KOH) was employed to enhance porosity development, increase nitrogen content, and minimize ash production, optimizing the adsorbent's structural and functional properties [16].

Materials and Methods

Materials

High purity gases (99.99%) were purchased from Roham gas company, Iran. All of the purchased chemicals were made by Merck Company with a purity of over 99%.

Fabrication of AC and CMS

To conduct the carbonization process [17], olive kernels were first crushed, ground, and sieved to obtain particle sizes ranging from 1 to 2 mm. The material was then subjected to thermal treatment at 840 °C for 1 hour under a continuous flow of nitrogen to achieve carbonization.

To eliminate impurities, the carbonized samples were washed with 100 mL of 0.1 M HCl, followed by thorough rinsing with distilled water until a neutral pH was attained. Subsequently, potassium hydroxide (KOH) was added to the carbonized material at a weight ratio of 2:1, and the mixture was heated at 80-90 °C for 6 hours. The optimal weight ratio was determined through preliminary experiments to achieve maximum SBET and pore size efficiency.

Finally, the samples were dried at 120 °C for 30 minutes, followed by heating at 300°C for 3 hours, and then carbonized at 800 °C, 700 °C, and 600 °C for 2 hours to obtain the AC1, AC2, and AC3 samples, respectively.

Fabrication of Carbon Molecular Sieve Samples

Each carbonized olive kernel sample (AC1, AC2, and AC3) was separately mixed with 1 g of powdered bitumen, impregnated with 5–6 mL of benzene solvent, and combined with 0.22 g of starch along with a few drops of water. In addition, the mixture was thoroughly blended and heated to 70–100 °C to evaporate the water, followed by drying at 100 °C.

To form tablets, the dried mixture was compressed at 10 bar and further dried in an oven at 100 °C for 2 hours. In the final stage of the calcination process, the tablets were crushed into powder and calcined in a horizontal furnace at 450 °C for 4 hours. The resulting products, CMS1, CMS2, and CMS3, were obtained.

Characterization

The Brunauer-Emmett-Teller (BET) test is essential for characterizing activated carbon, carbon molecular sieves (CMS), and other carbonaceous materials, playing a crucial role in adsorption studies and material engineering. It accurately determines specific surface area, a key factor in adsorption efficiency, and provides insights into pore size distribution, helping optimize materials for gas separation, catalysis, and filtration. Additionally, BET classifies adsorption isotherms, which aids in the design of catalysts, storage systems, and filtration media. Additionally, it ensures maximum adsorption efficiency in industrial applications like purification, air separation, and water treatment. By facilitating quality control and material comparisons, BET allows researchers to refine structural modifications for enhanced performance. As a non-destructive and highly reproducible method, BET delivers precise and reliable results, making it indispensable for developing high-performance carbon materials suited for environmental and energy applications.

The N2 adsorption and desorption isotherms were measured using Micromeritics C20 instruments, USA, at 77 K for all samples are shown in Fig. 1. The BET method was used to determine the specific surface area and pore volume of the samples, as shown in Table 1.

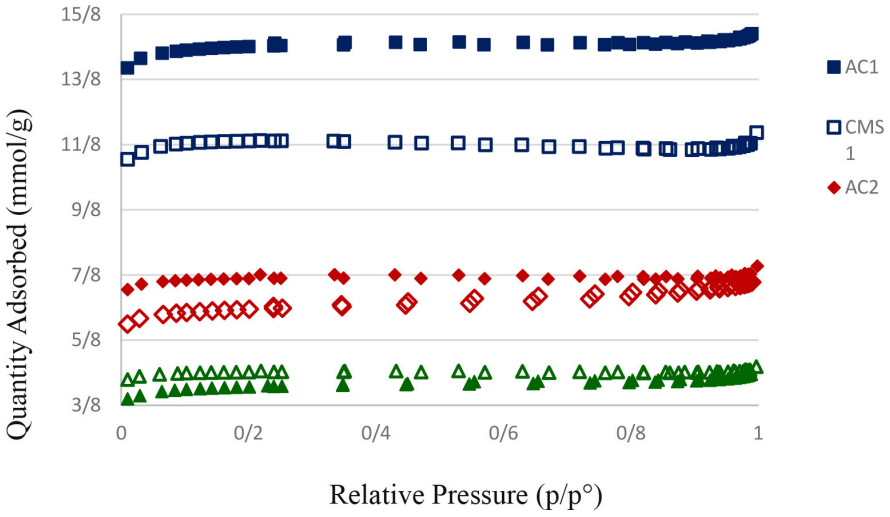

Fig. 1 N2 adsorption/desorption isotherms at 77 K.

Table 1 BET specific surface area of the samples.

Sample No.	AC1	AC2	AC3	CMS1	CMS2	CMS3
BET surface area (m^2/gr)	1103.92	572.80	327.55	888.28	503.96	360.79
(Pore volume (cm^2/gr	0.582	0.224	0.105	0.434	0.178	0.123

Adsorption Setup

Determining equilibrium data is imperative for designing adsorbent-based separation processes. In the laboratory, volumetric or gravimetric methods are the most commonly used methods for measuring the gas storage capacity of an adsorbent. In the gravimetric method, the adsorption equilibrium is determined based on the weight changes of the adsorbent during the gas adsorption process. Moreover, in the volumetric method, the difference in gas pressure before and after the adsorption process is measured. Furthermore, a schematic diagram of the adsorption process setup is shown in Fig. 2.

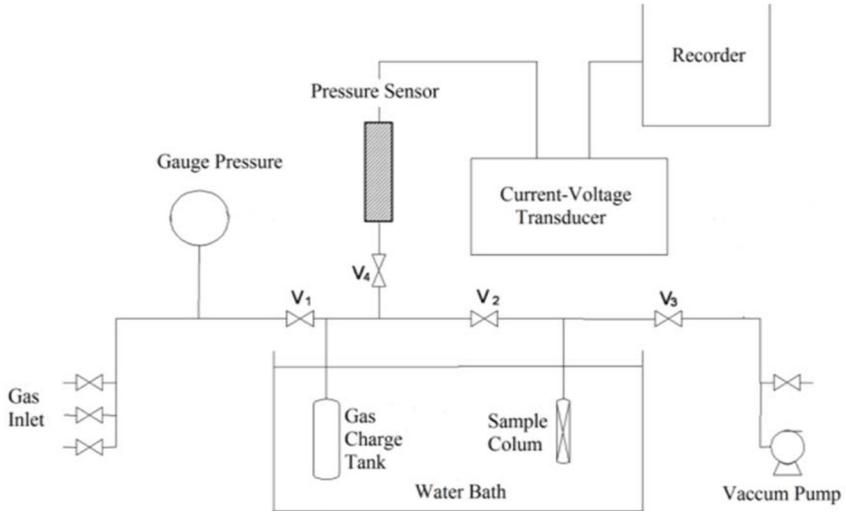

Fig. 2 Schematic diagram of the adsorption process setup.

As illustrated in Figure 2, the apparatus consists of two tanks: one designated for loading the adsorbed gas and the other serving as an absorbent container. A water bath is incorporated to regulate the desired temperature. In addition, the system utilizes a valve and pressure gauge to apply the required pressure to the gas tank, with real-time pressure readings provided by a high-precision sensor (accuracy: 0.0001 bar), which can be monitored via a connected computer. Additionally, a high-capacity vacuum pump is employed to degas the adsorbent samples, ensuring optimal performance. Furthermore, all structural components, including pipes, valves, fittings, and gas tanks, are constructed from steel, enabling the device to withstand a maximum pressure of 60 bar, ensuring durability and reliability in experimental applications.

Results and Discussion

Since this study focuses on the adsorption and separation of CO_2 and CH_4, the combined analysis of BET-derived data and results from the custom-built static adsorption setup (Fig. 2) offers valuable insights into the adsorption rates of these gases, enabling a comprehensive comparative evaluation.

Adsorption operates through three fundamental mechanisms: steric exclusion, kinetic selectivity, and equilibrium-based partitioning. Moreover, the steric effect, characteristic of molecular sieve materials such as zeolites, is dictated by the geometric constraints of the adsorbent's pore structure, allowing selective permeation based on molecular dimensions and shape. Moreover, molecules exhibiting appropriate size and symmetry can penetrate the adsorbent, whereas larger or structurally irregular molecules are excluded due to spatial limitations.

Kinetic separation, predominantly observed in carbon molecular sieves, arises from disparities in molecular diffusion rates within the porous medium. The variation in pore size distribution of carbon molecular sieves affects the relative penetration rates of different gas molecules, resulting in selective adsorption based on diffusion kinetics.

Equilibrium-driven adsorption mechanisms, which govern numerous adsorption phenomena, are dictated by thermodynamic interactions between the adsorbate and the adsorbent surface. In this investigation, experimental adsorption data analyzed using Langmuir, Freundlich, and Sips models revealed conformity with the Sips adsorption isotherm, substantiating the predominance of the kinetic mechanism in the observed adsorption behavior.

Since this study focuses on the adsorption and separation of CO_2 and CH_4, the combined analysis of BET-derived data and results from the custom-built static adsorption setup (Fig. 2) offers valuable insights into the adsorption rates of these gases, enabling a comprehensive comparative evaluation.

Furthermore, CO_2 and CH_4 adsorption isotherms were obtained for activated carbon and carbon molecular sieve samples at a temperature of 298 K (Fig. 3). Moreover, the adsorption tests were performed in the pressure range of 5 to 35 kPa. In addition, according to the IUPAC classification, all curves are of type I, in which case the gas adsorption increases with increasing pressure until it reaches the highest adsorption capacity of the adsorbent.

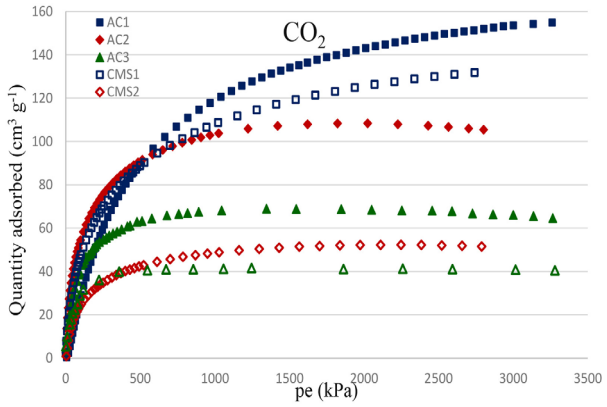

Fig. 3 CO_2 adsorption isotherms of the samples (Adsorbed volume/ Sorbent weight).

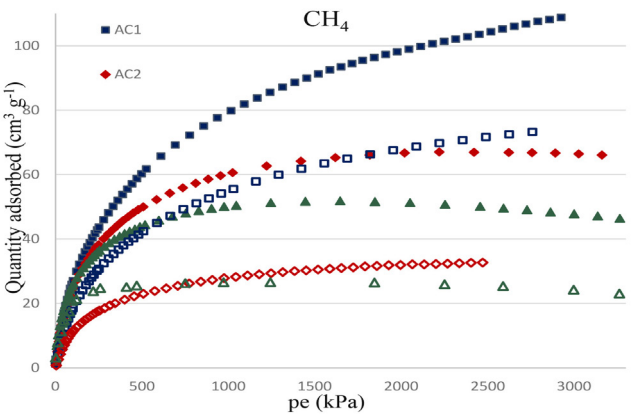

Fig. 4 CH_4 adsorption isotherms of the samples (Sorbate volume/ Sorbent weight).

After that, increasing the pressure does not affect the adsorption rate because the adsorbent is almost saturated. For activated carbon samples, the CO_2 gas adsorption rate was higher than that of CH_4. Additionally, the AC1 sample exhibited the highest gas adsorption rate, while CMS3 had the lowest. Furthermore, this indicates that the pore volume in this sample was higher than that of the other samples, and increasing the carbonization temperature had a significant effect on increasing the porosity of the samples; consequently, it can adsorb a larger volume of CO_2 gas. In addition, the SBET for the AC1 sample was 1103.92, indicating that the number of non-microporous pores and the required space for adsorption by more pores have increased, while the hindering factors of the adsorbent have decreased. Therefore, more gas was adsorbed, and the screening property and selectivity of the activated carbon decreased.

As shown in Fig. 1, the nitrogen adsorption/desorption isotherms are reversible for all samples, even though the adsorption desorption behaviors are not distinguishable due to the wide scale of the Y axis, and a hysteresis loop has not formed. Therefore, according to the IUPAC classification, the nitrogen adsorption isotherms are of type I [18]. Type I isotherms indicate that the samples are composed of micro-pores, and at low pressures, gas adsorption reaches its final value. Subsequently, the increase becomes very slight and almost constant. Most of the nitrogen adsorption has occurred at relatively low pressures, after which the graph becomes flat. According to Table 1, the highest BET surface area obtained is for the AC1 sample, and the lowest is for the AC3 sample.

As shown in Fig.s 3 and 4, due to the steric effect, a sudden drop (peak of the graph) was observed at the end of the adsorption processes for AC2, AC3, CMS2, and CMS3. Furthermore, CO_2 (Fig. 3) and CH4 (Fig. 4) adsorption on AC3 and CMS3 samples was more intense, whereas on AC2 and CMS2 samples, the steric effects were less pronounced. In addition, because of the formation of weak bonds between the sorbent and CO_2, this steric effect prevents the movement of the adsorbed molecules on the adsorbent. Thus, despite the pressure increase, the adsorption volume decreased. By considering CH_4 adsorption in the pressure range of 1200-1500 kPa, where an increase in the adsorption volume should be observed, a decrease in the amount of adsorption has occurred.

By comparing the results, it can be concluded that the steric effect has a greater impact on the CH_4 adsorbate.

Increasing pressure at specific temperatures in methane adsorption experiments results in a gradual enhancement of the adsorbent's capacity. Also, this highlights the significant influence of pressure on methane adsorption, despite the adsorbent's inherently low affinity for methane. Furthermore, operating conditions directly impact the adsorption rate, affecting overall performance. Moreover, equilibrium isotherm curves demonstrate that adsorbents exhibit a much greater tendency to adsorb CO_2 than CH_4. Additionally, due to its polarity, CO_2 strongly interacts with cationic surfaces, thereby facilitating adsorption. In contrast, methane, being a non-polar molecule, lacks a net dipole moment, resulting in weak interactions with cationic surfaces and a lower adsorption tendency [19]. Activation with oxygen-containing functional groups makes the surface of the adsorbent polar with a greater tendency to adsorb polar gases.

Langmuir and Freundlich, and Sips Isotherms

As discussed in reference [20], which builds upon prior published research, this topic has been previously examined. In that study, experimental adsorption values were evaluated using pseudo-first-order and second-order kinetic models, with corresponding adsorption constants determined.

However, the primary objective of this investigation is distinct, focusing exclusively on the fabrication of a carbon molecular sieve derived from olive kernel waste. Furthermore, it examines the impact of potassium hydroxide on its efficiency in selectively separating carbon dioxide from methane.

Various mathematical models have been developed to characterize gas adsorption behavior and equilibrium on solid adsorbent surfaces. Among these, the Langmuir and Freundlich models are widely employed for adsorption isotherm calculations. The Langmuir equation specifically describes surface adsorption phenomena, particularly chemical adsorption. In addition, it is based on several key assumptions, including monolayer adsorption, absence of interactions between adsorbed molecules, and surface homogeneity. Additionally, the Langmuir model follows kinetic principles, where equilibrium is attained when the adsorption rate equals the desorption rate [21].

The Langmuir equation is presented in Equation 1, where q is the amount of adsorbed gas at pressure p, q_m is the maximum adsorption capacity, and b is the Langmuir constant representing the adsorption energy.

$$\theta = \frac{q}{q_m} = \frac{bq}{1+bq} \quad (1)$$

Unlike Langmuir, the Freundlich adsorption isotherm is generally given as an empirical equation and assumes a heterogeneous surface and multilayer adsorption with a non-uniform distribution of heat of adsorption, and unlike Langmuir isotherm, it does not end in an adsorption limit. Moreover, the Freundlich isotherm is expressed as Equation 2:

$$q=k*p^{1/n} \quad (2)$$

Recognizing the increase in adsorption with rising concentration (pressure) in the Freundlich equation, Sips introduced an empirical model (Eq. 3) that closely resembles the Freundlich equation. However, like the Langmuir equation, the Sips model is based on monolayer adsorption, with the key distinction being the parameter n. In addition, when n = 1, the equation simplifies to the Langmuir model, which is suitable for homogeneous surfaces. Typically, when n exceeds 1, it indicates greater surface heterogeneity, with higher values corresponding to increased system inhomogeneity.

$$q = q_s * \frac{(bp)^n}{1+(bp)^n} \quad (2)$$

where q_s (cm^2/g) is the maximum capacity of adsorbed gas per gram of adsorbent; P (kPa) is the pressure of the gas; b is the affinity constant, which is related to the apparent energy of adsorption; n and K constants depend on the nature of the gas. In this study, all three models were used to describe experimental data obtained at a temperature of 298 K for the activated carbon and carbon molecular sieve samples. The results obtained for CO_2 and CH_4 gases for activated carbon (AC1-AC3) and carbon molecular sieve (CMS1-CMS3) samples by Langmuir, Freundlich, and Sips (Langmuir-Freundlich) models are given in Table 2. Moreover, the parameters and regression coefficients have been calculated using the relevant mathematical methods.

Langmuir, Freundlich, and Sips adsorption isotherms are plotted for CO_2 and CH_4 gases on both activated carbon and carbon molecular sieve samples (Fig.s 5-10). As shown in Tables 2, 3, and 4, the coefficient of determination (R^2) for all samples is greater than 0.93; however, this value is significantly better for the Sips isotherm compared to the Langmuir and Freundlich models. This means that the equilibrium adsorption data fits very well into the Sips equation.

Selectivity

To investigate the selectivity of the samples, experiments were conducted on a mixture of CO_2 and CH_4. Also, the Ideal Adsorbed Solution Theory (IAST) [22] and extended Langmuir (EL) [23, 24] theoretical models were used. The fitted parameters obtained from the Langmuir isotherm data of pure CO_2 and CH_4 gas were used for the models.

$$EL\ selectiviy = \frac{q_{si} * b_i}{q_{sj} * b_j} \quad (4)$$

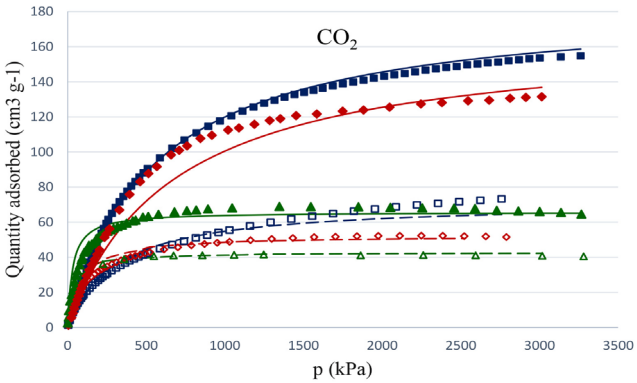

Fig. 5 Langmuir equation for CO_2 adsorption isotherms on activated carbon and carbon molecular sieve samples.

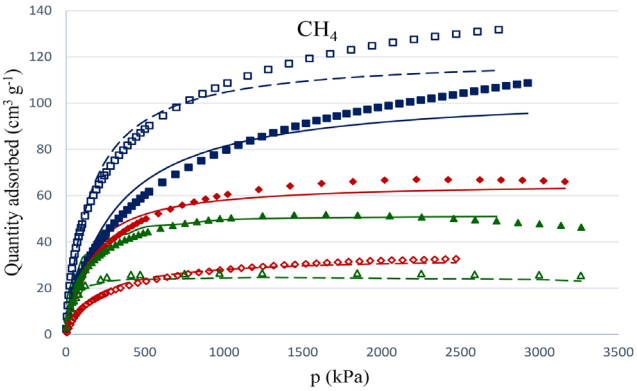

Fig. 6 Langmuir equation for CH_4 adsorption isotherms on activated carbon and carbon molecular sieve samples.

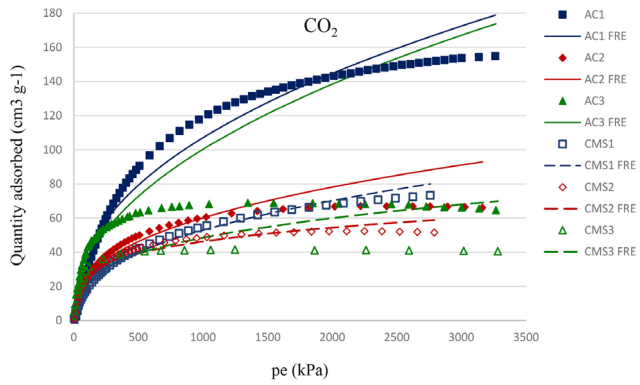

Fig. 7 Freundlich equation for CO_2 adsorption isotherms on activated carbon and carbon molecular sieve samples.

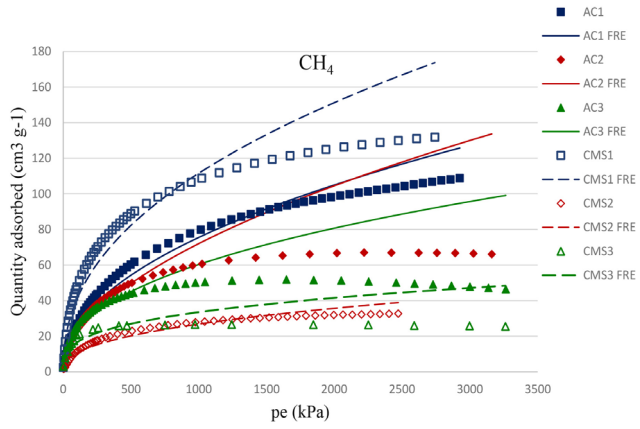

Fig. 8 Freundlich equation for CH_4 adsorption isotherms on activated carbon and carbon molecular sieve samples.

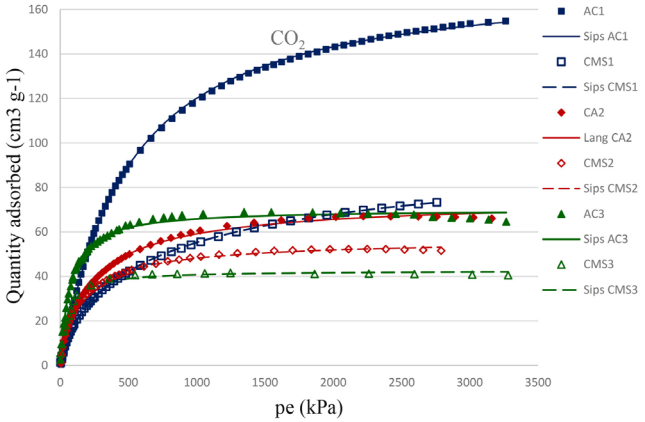

Fig. 9 Sips equation for CO_2 adsorption isotherms on activated carbon and carbon molecular sieve samples.

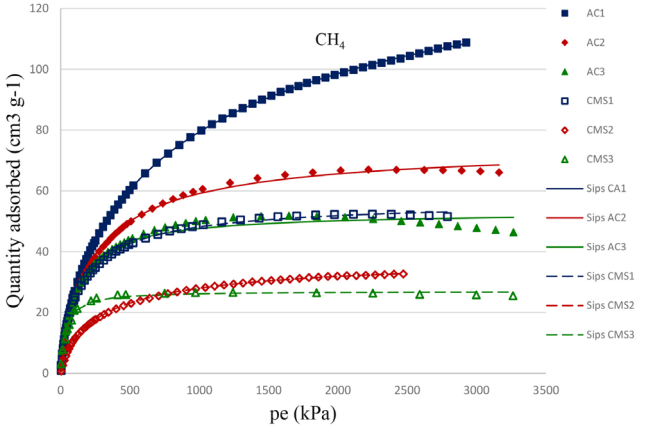

Fig. 10 Sips equation for CH_4 adsorption isotherms on activated carbon and carbon molecular sieve samples.

Table 2 Langmuir equation parameters for CO_2 and CH_4 gas adsorption on the samples.

	CO_2			CH_4		
Sample	b	Q	R2	b	Q	R2
AC1	0.001836	185.1852	0.9987	0.003390	105.2632	0.9806
AC2	0.003299	71.4286	0.9858	0.006585	120.4819	0.9752
AC3	0.007445	66.2250	0.9850	0.007495	65.7895	0.9991
CMS1	0.009745	52.5762	0.9961	0.005149	33.4448	0.9998
CMS2	0.032081	65.7895	0.9870	0.009481	52.6316	0.9861
CMS3	0.019744	42.9184	0.9931	0.007957	27.6243	0.9755

Table 3 Freundlich equation parameters for CO_2 and CH_4 gas adsorption on samples.

	CO_2			CH_4		
Sample	K	N	R2	K	N	R2
AC1	5.35698	2.30627	0.9510	2.8233	2.1022	0.9815
AC2	3.17244	2.45459	0.9851	5.3613	2.2758	0.9444
AC3	4.41541	2.64550	0.9560	1.7575	1.8605	0.9408
CMS1	9.16599	4.26803	0.9267	1.5641	2.4307	0.9340
CMS2	4.07104	2.15564	0.9336	3.3161	2.3815	0.9620
CMS3	5.83690	3.26158	0.9355	3.9674	3.2352	0.9073

Table 4 Sips equation parameters for CO_2 and CH_4 gas adsorption on samples.

	CO_2				CH_4			
Sample	N	b	qs	R^2	N	b	q_s	R^2
AC1	1.060	0.00147	174.10	0.9996	0.6851	0.0083	163.60	0.9995
AC2	0.720	0.00769	105.00	0.9998	0.8611	0.0138	57.26	0.9982
AC3	0.884	0.00811	75.38	0.9983	0.8837	0.0081	75.38	0.9982
CMS1	0.611	0.01380	57.26	0.9982	0.8083	0.0095	39.06	0.9996
CMS2	1.041	0.01183	70.00	0.9928	0.9287	0.0136	53.32	0.9834
CMS3	1.024	0.01898	42.59	9855 .0	1.0750	0.0200	26.93	0.9804

Using MATLAB software, the IAST model was applied to a binary mixture of CO_2 and CH_4. The results obtained from the IAST and EL models for an equimolar mixture of CO_2 and CH_4 in the pressure range of 0 to 41 bar are shown in Fig. 11.

According to both the IAST and EL models, AC1-AC3 were not suitable for CO_2 adsorption from the CH_4/CO_2 mixture. In other words, their adsorption was not selective. Moreover, CMS1-CMS3 has a selectivity greater than 2 and can therefore be used in pressure swing adsorption (PSA) operations. Furthermore, the selectivity of all three samples increased with pressure increase. As expected, at very low pressures, the selectivity by the IAST model approached the EL outcome (Table 5).

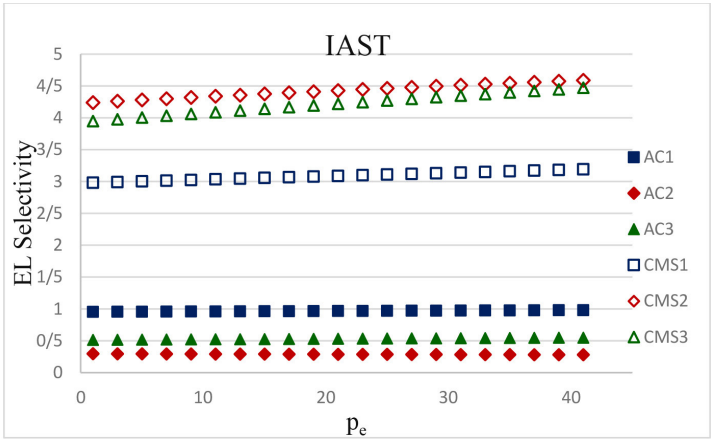

Fig. 11 IAST and EL models for an equimolar mixture of CO_2 and CH_4.

Table 5 EL selectivity

Sample	CO_2		CH_4		EL selectivity
	B	Qs	B	Qs	
AC1	0.001836	185.185	0.003390	105.2632	0.9528010
AC2	0.003299	71.428	0.006586	120.4819	0.2970115
AC3	0.007445	66.225	0.007495	65.7895	0.5141128
CMS1	0.009745	52.576	0.005149	33.4450	2.9751940
CMS2	0.032081	65.789	0.009481	52.6316	4.2296114
CMS3	0.019740	42.918	0.007957	27.0620	3.9343897

Among the carbon molecular sieve samples, the order of CO_2 adsorption was CMS1> CMS2> CMS3. This trend is consistent with the BET results. While for methane, CMS1 had the highest adsorption (similar to CO_2 adsorption), CMS2 and CMS3 showed almost the same result (the adsorption of CMS2 was slightly higher than that of CMS3). Additionally, this may be attributed to the smaller diameter of the dioxide molecules (0.33 nm vs. 0.38 nm) and the sieving property of the adsorbents. Consequently, Carbon dioxide molecules had easily passed through the larger pores of the CMS1. At the same time, the steric mechanism prevails for CMS2 and CMS3. Regarding the activated carbon samples, the adsorption order is as follows:

For CO_2: AC1> AC2≈ AC3

For CH_4 AC1 > AC2 ≈ AC3

For these samples, the adsorption rates of both molecules are consistent with the BET specific surface areas. It should be noted that for the carbon molecular sieve and activated carbon samples, the adsorption of carbon dioxide molecules was higher than that of methane, which is due to the nonpolar character of the methane molecule and the cationic nature of the adsorbent, which has a greater tendency to adsorb polar molecules.

The results show that increasing the carbonization temperature increases the BET surface area, resulting in a higher rate of gas adsorption on the adsorbent, particularly for CO_2. Moreover, calcination of activated carbon samples reduces the surface area of the samples and reduces the rate of adsorption, while the selectivity of the adsorbent for gas adsorption increases significantly.

Conclusions

This study systematically investigated the synthesis of carbonaceous adsorbents—activated carbon (AC) and carbon molecular sieve (CMS)—derived from olive kernels through the optimization of key parameters, including carbonization temperature, chemical activating agent, and weight ratio. Moreover, gas adsorption experiments for CO_2 and CH_4 revealed a pronounced preference for CO_2 adsorption, with samples carbonized at 800 °C exhibiting superior adsorption capacity and specific surface area. Among the adsorbents, CMS demonstrated enhanced CO_2-CH_4 separation efficiency, with the Sips model providing the highest correlation with equilibrium data.

The selectivity indices for CMS2 and CMS3 were notably high, particularly at 800 °C, where CO_2 adsorption was augmented by polarization effects induced by the hydroxide activating agent. This polarization strengthened the interaction between CO_2 molecules and the adsorbent, overcoming steric hindrance effects associated with larger CH_4 molecules. While activated carbon exhibited diminished molecular sieving properties at elevated temperatures, it remained a viable option for light gas separation under lower temperature and pressure conditions, offering a cost-effective solution with a high specific surface area per unit mass.

In conclusion, CMS proved to be more efficient than activated carbon for CO_2 separation from CH_4, particularly at high temperatures, due to its higher specific surface area and adsorption capacity. In addition, the study suggests that activated carbon, despite its limitations at high temperatures, remains a practical option for separating light gases due to its affordability and efficiency.

Acknowledgements
We thank the Research Institute of Petroleum Industry (R.I.P.I.) for its support of this work.

References

1. Sircar, S., Golden, T. C., & Rao, M. B. (1996). Activated carbon for gas separation and storage. Carbon, 34(1), 1-12. doi.org/10.1016/0008-6223(95)00128-X.
2. Djeridi, W., Ouederni, A., Wiersum, A. D., Llewellyn, P. L., & El Mir, L. (2013). High pressure methane adsorption on microporous carbon monoliths prepared by olives stones. Materials Letters, 99, 184-187. doi.org/10.1016/j.matlet.2013.03.044.
3. Kabeyi, M. J. B., & Olanrewaju, O. A. (2022). Biogas production and applications in the sustainable energy transition. Journal of Energy, 2022(1), 8750221. doi.org/10.1155/2022/8750221.
4. Wang, Q., Luo, J., Zhong, Z., & Borgna, A. (2011). CO_2 capture by solid adsorbents and their applications: current status and new trends. Energy & Environmental Science, 4(1), 42-55.
5. Sun, Q., Li, H., Yan, J., Liu, L., Yu, Z., & Yu, X. (2015). Selection of appropriate biogas upgrading technology-a review of biogas cleaning, upgrading and utilisation. Renewable and Sustainable Energy Reviews, 51, 521-532. doi.org/10.1016/j.rser.2015.06.029.
6. Ngo, T. C. Q., Tran, T. K. N., Chau, H. D., & Hoang, B. N. (2023). The material potential and application of activated carbon from nut shells: Mini review. Materials Today: Proceedings. doi.org/10.1016/j.matpr.2023.03.511.
7. Shabi, A. H., Prima Hardianto, Y., Shaheen Shah, S., Omar Al-Qwairi, F., Mohamed, M. M., Nasiruzzaman Shaikh, M., Saeed Alzahrani, A. & Aziz, M. A. (2024). Advancements in olive-derived carbon: preparation methods and sustainable applications. Chemistry–An Asian Journal, 19(8), e202400045. doi.org/10.1002/asia.202400045.
8. Aimikhe, V. J., Anyebe, M. S., & Ibezim-Ezeani, M. (2024). Development of composite activated carbon from mango and almond seed shells for CO_2 capture. Biomass Conversion and Biorefinery, 14(4), 4645-4659. doi.org/10.1007/s13399-022-03665-w.
9. Bartucci, S., Poselle Bonaventura, C., Pace, L., Conte, G., Desiderio, G., Mintova, S., Agostino, R.G. & Policicchio, A. (2024). Peach pit-activated carbons: effect of row material form and pyrolysis parameters on hydrogen adsorption storage. ACS Applied Engineering Materials, 2(4), 853-867. doi.org/10.1021/acsaenm.3c00733.
10. Michałek, T., Wojtaszek, K., Małecki, S., Kornaus, K., Wandor, S., Druciarek, J., Fitzner, K. and Wojnicki, M., 2023. Recovery of Pd (II) ions from aqueous solutions using activated carbon obtained in a single-stage synthesis from cherry seeds. C, 9(2), p.46. doi.org/10.3390/c9020046.
11. Aouay, F., Attia, A., Dammak, L., Ben Amar, R., & Deratani, A. (2024). Activated carbon prepared from waste coffee grounds: Characterization and adsorption properties of dyes. Materials, 17(13), 3078. doi.org/10.3390/ma17133078.
12. Silva, M. C., Crespo, L. H., Cazetta, A. L., Silva, T. L., Spessato, L., & Almeida, V. C. (2024). Activated carbon fibers of high surface area from corn husk: Mono and multicomponent adsorption studies of Pb2+ and Cu2+ ions from aqueous solution. Journal of Molecular Liquids, 405, 124919. doi.org/10.1016/j.molliq.2024.124919.
13. Metyouy, K., Benkirane, L., Sánchez, M. E., Cara-Jiménez, J., Plakas, K. V., & Chafik, T. (2024). Valorization of agricultural olive waste as an activated carbon adsorbent for the remediation of water sources contaminated with pharmaceuticals. Sustainable Chemistry for the Environment, 6, 100110. doi.org/10.1016/j.scenv.2024.100110.
14. Monteagudo, J. M., Durán, A., Alonso, M., & Stoica, A. I. (2025). Investigation of effectiveness of KOH-activated olive pomace biochar for efficient direct air capture of CO_2. Separation and Purification Technology, 352, 127997. doi.org/10.1016/j.seppur.2024.127997
15. Dissanayake, P. D., You, S., Igalavithana, A. D., Xia, Y., Bhatnagar, A., Gupta, S., Kua, H.W., Kim, S., Kwon, J.H., Tsang, D.C. & Ok, Y. S. (2020). Biochar-based adsorbents for carbon dioxide capture: A critical review. Renewable and Sustainable Energy Reviews, 119, 109582. doi.org/10.1016/j.rser.2019.109582.
16. Williams, N. E., Oba, O. A., & Aydinlik, N. P. (2022). Modification, production, and methods of KOH-activated carbon. ChemBioEng Reviews, 9(2), 164-189. doi.org/10.1002/cben.202100030.
17. Ubago-Pérez, R., Carrasco-Marín, F., Fairén-Jiménez, D., & Moreno-Castilla, C. (2006). Granular and monolithic activated carbons from KOH-activation of olive stones. Microporous and mesoporous materials, 92(1-3), 64-70. doi.org/10.1016/j.micromeso.2006.01.002.
18. Thommes, M., Kaneko, K., Neimark, A. V., Olivier, J. P., Rodriguez-Reinoso, F., Rouquerol, J., & Sing, K. S. (2015). Physisorption of gases, with special reference to the evaluation of surface area and pore size distribution (IUPAC Technical Report). Pure and Applied Chemistry, 87(9-10), 1051-1069.
19. Alcañiz-Monge, J., Lozano-Castelló, D., Cazorla-Amorós, D., & Linares-Solano, A. (2009). Fundamentals of methane adsorption in microporous carbons. Microporous and Mesoporous Materials, 124(1-3), 110-116. doi.org/10.1016/j.micromeso.2009.04.041.
20. Hanaor, D. A., Ghadiri, M., Chrzanowski, W., & Gan, Y. (2014). Scalable surface area characterization by electrokinetic analysis of complex anion adsorption. Langmuir, 30(50), 15143-15152. doi.org/10.1021/la503581e
21. Mousavi, Z., & Bozorgzadeh, H. R. (2017). Preparation of carbon molecular sieves from pistachio shell and walnut shell for kinetic separation of carbon monoxide, hydrogen and methane.
22. Walton, K. S., & Sholl, D. S. (2015). Predicting multicomponent adsorption: 50 years of the ideal adsorbed solution theory. AIChE Journal, 61(9), 2757-2762. doi.org/10.1002/aic.14878.
23. Zhang, P., & Wang, L. (2010). Extended Langmuir equation for correlating multilayer adsorption equilibrium data. Separation and Purification Technology, 70(3),

367-371. doi.org/10.1016/j.seppur.2009.10.007.
24. Swenson, H., & Stadie, N. P. (2019). Langmuir's theory of adsorption: A centennial review. Langmuir, 35(16), 5409-5426. doi.org/10.1021/acs.langmuir.9b00154.